Progressive Application of a Lagrangian Vortex Method into Fluid Engineering and Possibility of the Concept of Discrete Element Methods in Vortex Dynamics (Mathematical analysis of the Euler equations : 150 years of vortex dynamics)

AUTHOR(S):

Kamemoto, Kyoji

数理解析研究所講究録
第1642巻 2009年 53-66

Progressive Application of a Lagrangian Vortex Method into Fluid Engineering and Possibility of the Concept of Discrete Element Methods in Vortex Dynamics

Kyoji Kamemoto
Professor Emeritus, Department of Mechanical Engineering,
Yokohama National University

1. Introduction

The vortex methods have been developed and applied for analysis of complex, unsteady and vortical flows in relation to problems in a wide range of industries, because they consist of simple algorithm based on physics of flow. Nowadays, applicability of the vortex element methods has been developed and improved dramatically, and it has become encouragingly clear that the vortex methods have so much interesting features that they provide researchers and engineers with easy-to-handle and completely grid-free Lagrangian calculation of unsteady and vortical flows without use of any RANS type turbulence models. Leonard[1] summarized the basic algorithm and examples of its applications. Sarpkaya[2] presented a comprehensive review of various vortex methods based on Lagrangian or mixed Lagrangian-Eulerian schemes, the Biot-Savart law or the vortex in cell methods. Kamemoto[3] summarized the mathematical basis of the Biot-Savart law methods. Recently, Kamemoto[4] reported several attractive applications involving simulation of various kinds of unsteady flows with an advanced vortex method, and Ojima and Kamemoto[5] reported interesting results of a study on numerical simulation of unsteady flows around a swimming fish by using their vortex method.

As well as many finite difference methods, it is a crucial point in vortex methods that the number of vortex elements should be increased when higher resolution of turbulence structures is required, and then the computational time increases rapidly. In order to reduce the operation count of evaluating the velocity at each vortex element or particle through a Biot-Savart law, fast N-body solvers, by which the operation count is reduced from $O(N^2)$ to $O(N \log N)$, have been proposed by Greengard and Rohklin.[6] On the other hand, in order to reduce the computational load in calculation of turbulence structures, Fukuda and Kamemoto[7] proposed an effective redistribution model of vortex elements with consideration of convective motion and viscous diffusion in a three-dimensional core-spreading model.

Recently, in order to expand the applicability of the advanced vortex method, the group of the present author has made attempts to apply it into further complicated and vortical flows in several fields. Kamemoto and Ojima[8] applied the method into the fluid dynamics in sports science, and they simulated three-dimensional, complex and unsteady flows around an isolated 100 m runner and also a ski-jumper. Iso and Kamemoto[9] developed a coupled vortex method and particle method analysis tool for numerical simulation of internal unsteady two-phase flows, and they numerically simulated internal liquid-solid two-phase flows in a vertical channel and a mixing tee. Furthermore, expanding the concept of the Lagrangian vortex method in which vorticity layers are expressed by a number of discrete vortex elements, Ishimoto[10] and the group of the present author have attempted numerical simulation of behavior of plasma in a magnetic field by introducing superparticles of electrons.

In this paper, in order to overview the recent attempts, the mathematical background and numerical procedure of the advanced vortex method applied to the recent studies are briefly explained and the progressive studies on simulation of such hard-to-solve and vortical flows as the complex flows around a 100 m runner, the liquid-particle two phase flows in a

channel and the vortical motion of plasma clouds in a magnetic field are digested. And finally, a new direction of further development of the vortex element dynamics is viewed in conclusion.

2. Algorithms of Lagrangian Vortex Element Method

The governing equations for viscous and incompressible flow are described with the vorticity transport equation and the pressure Poisson equation, which can be derived by taking the rotation and the divergence of Navier-Stokes equations, respectively.

$$\frac{\partial \boldsymbol{\omega}}{\partial t} + (\boldsymbol{u} \cdot grad)\boldsymbol{\omega} = (\boldsymbol{\omega} \cdot grad)\boldsymbol{u} + \nu \nabla^2 \boldsymbol{\omega} \tag{1}$$

$$\nabla^2 p = \rho \, div(\boldsymbol{u} \cdot grad \, \boldsymbol{u}) \tag{2}$$

Where $\boldsymbol{u}$ is a velocity vector, and ν and ρ respectively denote kinematic viscosity and fluid density. The vorticity $\boldsymbol{\omega}$ is defined as $\boldsymbol{\omega} = rot\, \boldsymbol{u}$. As explained by Wu and Thompson1[11], the Biot-Savart law can be derived from the definition equation of vorticity as follows.

$$\boldsymbol{u} = \int_V (\boldsymbol{\omega}_0 \times \nabla_0 G) \, dv + \int_S \{(\boldsymbol{n}_0 \cdot \boldsymbol{u}_0) \cdot \nabla_0 G - (\boldsymbol{n}_0 \times \boldsymbol{u}_0) \times \nabla_0 \, G\} \, ds \tag{3}$$

Here, subscript "$_0$" in Eq.(3) denotes variable, differentiation and integration at a location $\boldsymbol{r}_0$, and $\boldsymbol{n}_0$ denotes the normal unit vector at a point on a boundary surface S. And G is the fundamental solution of the scalar Laplace equation with the delta function $\delta(\boldsymbol{r}-\boldsymbol{r}_0)$ in the right hand side, which is written as $G = 1/(4\pi|\boldsymbol{r}-\boldsymbol{r}_0|)$ for a three-dimensional field. In Eq. (3), the inner product ($\boldsymbol{n}_0 \cdot \boldsymbol{u}_0$) and the outer product ($\boldsymbol{n}_0 \times \boldsymbol{u}_0$) stand for respectively normal and tangential velocity components on the boundary surface, and they respectively correspond to source and vortex distributions on the surface. Therefore, as shown in Fig.1, it is mathematically understood that a velocity field of viscous and incompressible flow is arrived at the field integration concerning vorticity distributions in the flow field and the surface integration concerning source and vortex distributions around the boundary surface.

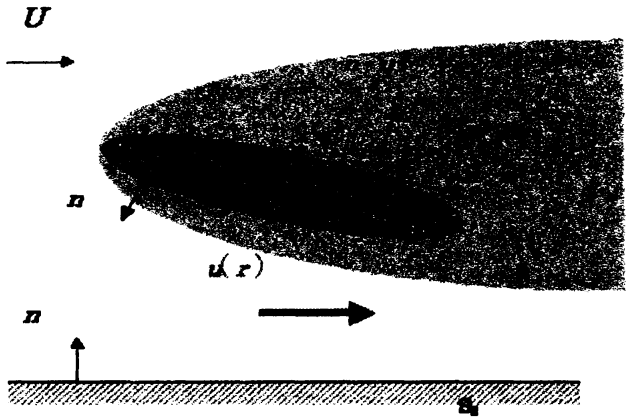

Fig. 1 Flow field involving vorticity distribution region.

Instead of the finite difference calculation of the pressure Poisson equation represented by Eq. (2), the pressure in the flow field is calculated from the integration equation, which was formulated by Uhlman[12] as follows.

$$\beta H + \int_S H \frac{\partial G}{\partial n} ds = -\int_V \nabla G (\boldsymbol{u} \times \boldsymbol{\omega}) dv - \int_S \left\{ G \cdot \mathrm{n} \cdot \frac{\partial \boldsymbol{u}}{\partial t} + \nu \cdot \mathrm{n} \cdot (\nabla G \times \boldsymbol{\omega}) \right\} ds \qquad (4)$$

Here, β is $\beta = 1$ inside the flow and $\beta = 1/2$ on the boundary S. H is the Bernoulli function defined as $H = P/\rho + |\boldsymbol{u}|^2/2$. The value of H on the boundary surface is calculated from Eq. (4) by using the panel method.

One of the most important schemes in the vortex method is how to represent the distribution of vorticity in the proximity of the body surface, taking account of viscous diffusion and convection of vorticity under the non-slip condition on the surface. In the present method, a thin vorticity layer is considered along the solid surface, and discrete vortex elements are introduced into the surrounding flow field considering the diffusion and convection of vorticity from discrete elements of the thin vorticity layer with vorticity $\boldsymbol{\omega}$. The details of treatments have been explained in the paper written by Ojima & Kamemoto [13]. It will be noteworthy that as a linear distribution of velocity is assumed in the thin vorticity layer, the frictional stress on the wall surface is evaluated approximately from the following equation as $\tau_w = \mu \partial \boldsymbol{u}/\partial n = -\mu \boldsymbol{\omega}$. Once the pressure distribution and frictional stress around the boundary surface are calculated, integration of the pressure and the shearing stress along the surface yields the force acting on the body. When a vortex element, which is introduced into the surrounding field, flows downstream and far from the solid surface, it can be replaced with an equivalent discrete vortex element for simplification of numerical treatment by considering conservation of vortex strength. The discrete vortex element is modeled by a vortex blob which has a spherical structure with a radial symmetric vorticity distribution proposed by Winkelmans & Leonard[14]. The motion of the discrete vortex elements is represented by Lagrangian form of a simple differential equation $d\boldsymbol{r}/dt = \boldsymbol{u}$. Then, trajectory of a discrete vortex element over a time step is approximately computed from the Adams-Bashforth method. On the other hand, the evolution of vorticity is calculated by Eq.(1) with the three-dimensional core spreading method proposed by Nakanishi & Kamemoto[15]. It should be noted here that in order to keep higher accuracy in expression of a local vorticity distribution, a couple of additional schemes of re-distribution of vortex blobs are introduced in the present advanced vortex method. When the vortex core of a blob becomes larger than a representative scale of the local flow passage, the vortex blob is divided into a couple of smaller blobs. On the other hand, if the rate of three-dimensional elongation becomes large to some extent, the vortex blob is discretized into plural blobs in order to approximate the elongated vorticity distribution much more properly. The detail of the redistribution model is explained in the paper written by Fukuda and Kamemoto[7].

3. Progressive Applications

3.1 Application to sports aerodynamics

In the study of numerical simulation of the flows around a 100 m runner and a ski-jumper by Kamemoto and Ojima[8], a numerical model of a moving athlete is represented by distributing 3,020 quadrilateral panels around its body-surface as shown in Fig.2 (a). For the moving conditions of each panel, the new co-ordinates of each panel, instantaneous velocity and acceleration of the panel movement are given at each time step, and the one cycle of motion is produced by 320steps of instantaneous body configuration as shown in Fig.2 (b) in

which only eight characteristic steps of instantaneous running style are shown. The moving boundary data are imported into the calculation at each time step, which are used to change both the configuration of athlete body and the boundary condition during the calculation of the flow field around the moving body. In order to examine the influence of runner's posture, calculations of flows around a runner with different forward-bent angles (α=0°, 10°, 20°, 30°) shown in Fig.2 (c) were performed. Moreover, a much more realistic flow around the runner was simulated by introducing continuous variation of the forward-bent angle from 50° to 0° degree with the elapsed time.

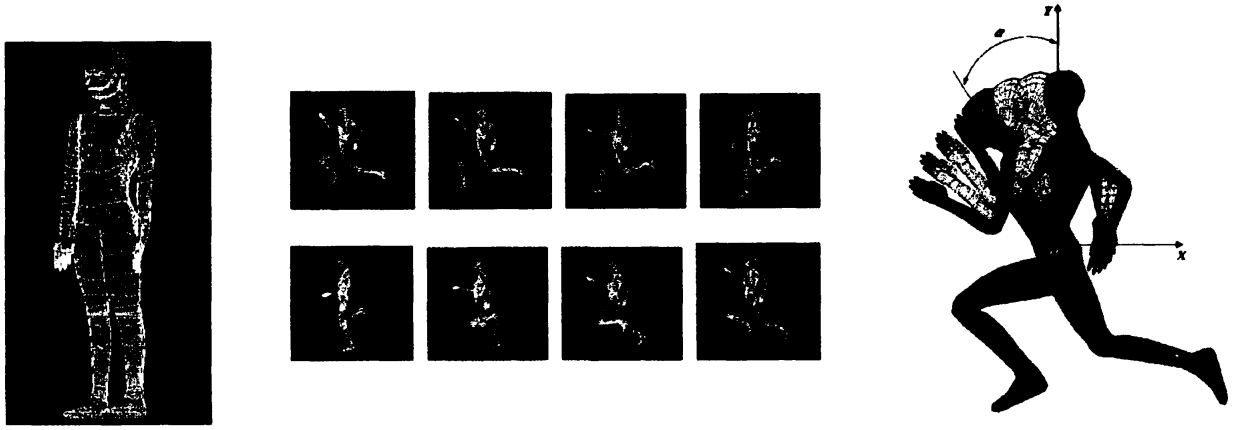

(a) Panel distribution (b) One cycle of running motion at α=0° (c) Definition of forward-bent angle α

Fig.2 Representation of a body configuration by quadrilateral panels.

In the study, in order to normalize length scale, the breadth of the runner's shoulders 0.4 m was used as the representative length L for normalization of the length scale. The assumed running speed 10 m/s was used as the representative velocity U for normalization of the velocity scale. As one cycle motion was represented 320 steps of instantaneous body configuration, and as it is known that one cycle of sprint running motion of a first class runner takes approximately 0.45 s, the size of time step of the present time marching calculations was taken to be 1.40×10^{-3} s. The kinematic viscosity ν and density ρ of the atmosphere were respectively assumed as 1.43×10^{-5} m^2/s and 1.2 kg/m^3. Therefore, the Reynolds number of the flow around the runner becomes $Re = UL/\nu = 2.8\times10^5$.

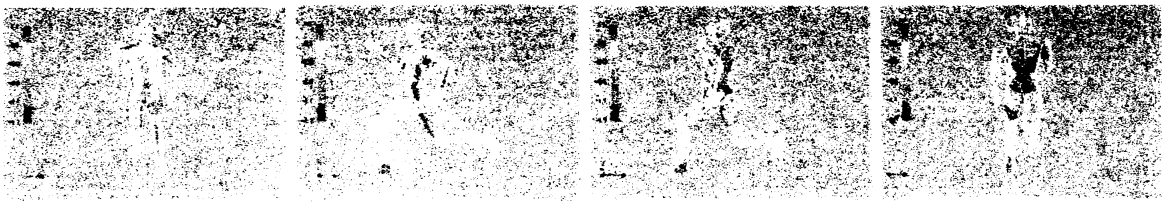

(a) Front view (b) Side view (c) Oblique view (d) Rear view

Fig. 3 An instantaneous pressure distribution around the runner's body surface at the bent angle α=0°.

Figure 3 shows four views of instantaneous pressure distributions around the runner's body surface at the bent angle α=0°. It is clearly observed that higher pressure regions are formed on the face and frontal surfaces of body and the left leg, and lower pressure spots are formed on the back and side surfaces of body and the rear surface of the left foot. And it has been known from the calculation that the time-averaged total drag force acting on the runner was

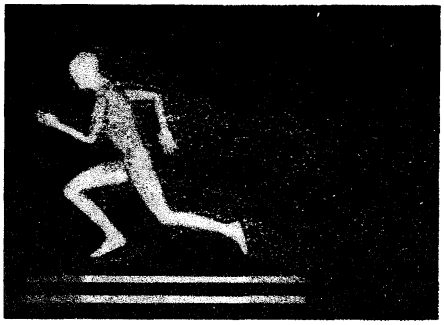

(a) t =1.8sec (α=30°)

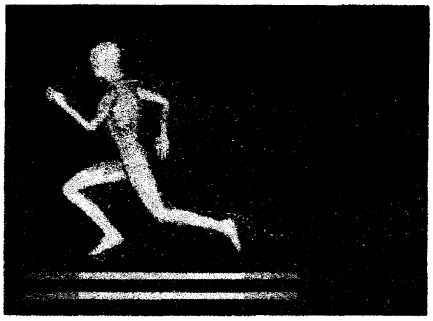

(b) t =2.7sec (α=20°)

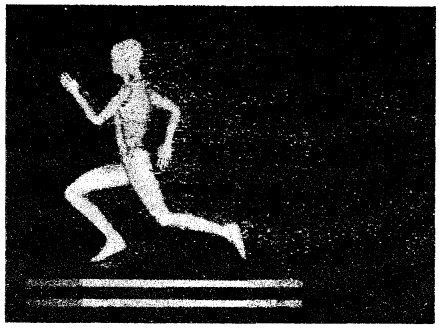

(c) t =3.6sec (α=10°)

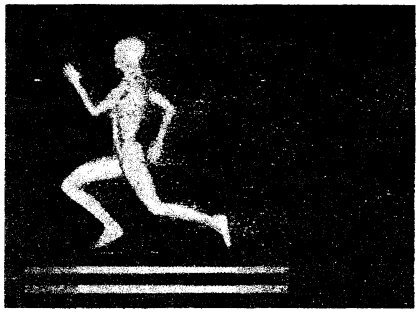

(d) t =4.5sec (α=0°)

Fig.4 Instantaneous pressure distributions and flow patterns around a runner changing the forward-bent posture.

about 18 N which corresponds to the value of drag coefficient Cd ~ 0.8 on the assumption of drag area as about 0.4 m^2.

Figure 4 shows instantaneous pressure distributions and flow patterns around a runner who is continuously changing forward-bent posture from 50° to 0°. It is seen in this figure that the width of the wake formed behind the runner at the forward-bent angle is 30° is narrower and it becomes wider as the forward-bent angle becomes smaller. It has been confirmed from this calculations that the fluid force acting on the runner varies according to the angle of forward-bent posture.

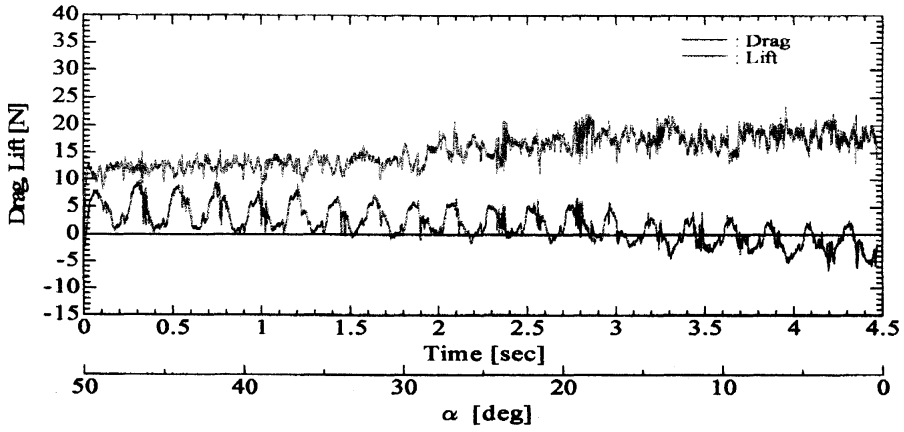

Fig.5 Time history of drag and lift forces during motion of continuously changing the forward-bent posture from 50° to 0° with time.

Figure 5 shows time history of drag and lift forces acting on the runner during motion of continuously changing the forward-bent posture from 50° to 0° with time. It is interesting to find that as the forward-bent angle decreases, drag force tends to increase monotonously and lift force is periodically fluctuating but it tends to decrease from positive lift (up-force) to negative one (down force).

3.2 Application of a coupled vortex element and particle method to liquid-solid two-phase flows

In the study by Iso and Kamemoto[9], both fluid phase and particle phase are treated by the completely grid-free Lagrangian-Lagrangian simulation, without use of the Eulerian grids as schematically shown in Fig.6. It is possible to simulate directly particle motion oriented by the vortex-induced fluid dynamical forces. Detail of the method and examples applied to internal multiphase flows are described in the paper by Iso and Kamemoto[16]. Solid particles were treated by the particle trajectory tracking method as a Lagrangian calculation. Particle-particle and particle-wall collisions are calculated by a deterministic method. To simplify the problem in this study, the liquid-solid two-phase flows are treated as those of dilute mixture of particles and it is assumed that the effect of particles on the liquid flow is neglected (one-way model). And a solid particles is considered as a rigid sphere with a particle diameter.

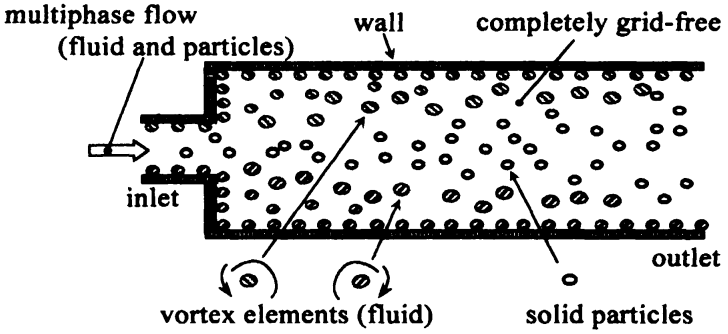

Fig. 6 Schematic diagram of numerical method of the present Lagrangian-Lagrangian simulation for internal flows.

Based on the above assumptions, it is generally accepted that dominant forces on each particle are the drag force, Magnus lift force, Saffman lift force, force to accelerate the virtually added mass in the ambient fluid, and gravitational force. The force on the particles due to pressure gradient and the Basset force are neglected in this study. The equation of motion for a particle is expressed as

$$\frac{d\boldsymbol{u}_p}{dt} = \frac{1}{M_p}\left(\boldsymbol{F}_D + \boldsymbol{F}_{LM} + \boldsymbol{F}_{LS} + \boldsymbol{F}_{VM} + \boldsymbol{F}_G\right) \tag{5}$$

Here, $\boldsymbol{u}_p$ is the particle velocity vector, M_p the particle mass, and $\boldsymbol{F}$ the force vector on the particle; namely, $\boldsymbol{F}_D$ is the drag force due to relative velocity of the particle to the fluid, $\boldsymbol{F}_{LM}$ the Magnus lift force due to rotational motion, $\boldsymbol{F}_{LS}$ the Saffman lift force due to velocity gradient, $\boldsymbol{F}_{VM}$ the force to accelerate the virtual added mass in the ambient fluid and $\boldsymbol{F}_G$ the gravitational force. In this paper, calculation formulas of the above forces on particles are

omitted. They are similar to the formulas in the literature, for example, Tsuji et al.[17] and Yamamoto et al. [18]

As the rotation of a particle is affected by the fluid viscosity, the equation of rotational motion of each particle is numerically solved by considering the viscous torque against particle rotation which is theoretically obtained by Dennis et al.[19].

Particle-particle and particle-wall collisions were calculated by a deterministic method. The traveling velocity and the rotational velocity of a particle after collision are calculated by the equations of impulsive motion of a particle. For the calculation of particle-wall collision, the collision is modeled as irregular bouncing of a particle on the virtual wall model proposed by Tsuji et al.[17], in which the wall is replaced with a virtual wall having an angle relative to the real wall.

Physical motion of the particles is split up into two stages in order to reduce the computational load. In the first stage, all particles are moved based on the equation of motion without collisions. In the second stage, particle-particle collision is calculated, and then, the velocity of a particle after the collision is replaced with post-collision velocity without changing the position.

In the beginning, the two-dimensional liquid-solid two-phase flow in a vertical channel was calculated to validate the coupled vortex element and particle method. The numerical simulation was performed for the same conditions as those in the two-phase experiments of Hishida et al. [20, 21]. The flow field is schematically shown in Fig.5. Flow direction of both phases is downwards. The Reynolds number is $R_e = U_c W / \nu = 5.0\times10^3$, based on the mean velocity on the centerline U_c =0.17 m/s and the channel width $W=3.0\times10^{-2}$ m. Here, ν is the kinematic viscosity of water. Periodic boundary conditions for both phases were applied in the streamwise direction due to restrictions on computational power. The length L of the computational region in the streamwise direction was equal to $3W$. Particles are introduced into the channel using random numbers, so as to satisfy uniform distribution at the loading mass ratio which is $m=1.1\times10^{-2}$. Density and diameter of the particles are ρ_p =2590 kg/m^3 (relative density: ρ_p/ρ_f= 2.59) and d_p=500μm, respectively.

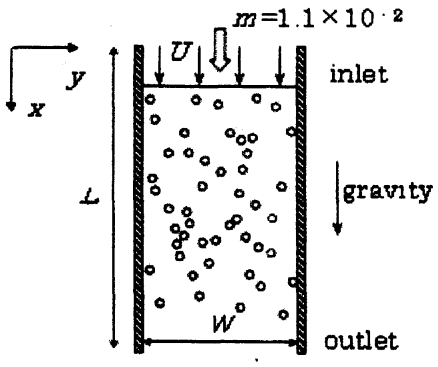

Fig. 7 Schematic view of liquid-solid two phase flow in a vertical channel.

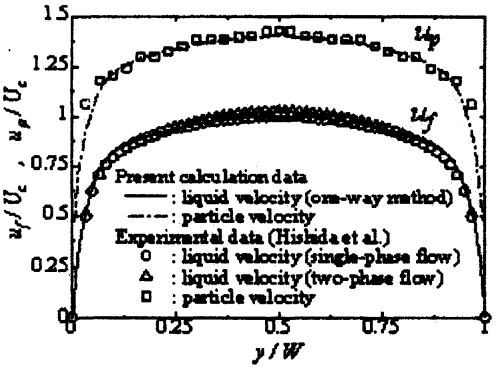

Fig. 8 The time-averaged streamwise velocities of fluid and solid particles.

Figure 8 shows the results for the time-averaged streamwise velocities of fluid and solid particles. In this downward flow, the particle velocity is faster than the liquid, because the density of particles is larger. Numerical results showed very good agreement with the experimental data of Hishida et al. [20, 21]. As the conclusion, these validations clarified the

quantitative accuracy and the applicability of the special combination of vortex method and particle trajectory tracking method to internal two-phase flow of high Reynolds number.

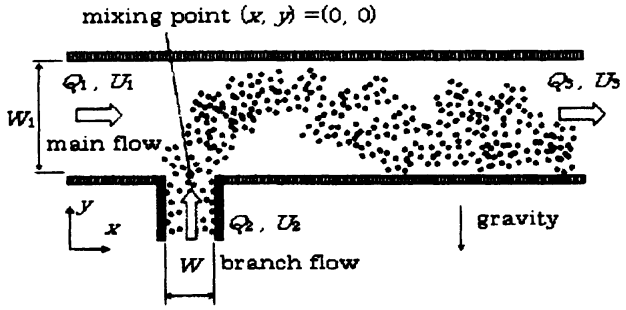

Fig.9 Schematic view of the liquid-solid two-phase flow in the mixing tee.

The coupled vortex element and particle method was applied to the two-dimensional liquid-solid two-phase flow in a mixing tee as a typical problem to mixing of liquid and solid particles in ducts. The flow field is schematically shown in Fig.9. The flow field is not only the basic component in industrial pipelines but also the simple mixing device for multi-phase flow. For details, refer to Kawashima et al.[22, 23] and Blancard et al.[24]. In Fig.9, the branch flow merges into the main flow at a right angle. The cross-sections of the confluence are squares. The widths of the main and branch channels are W_1 and W_2, respectively, and the width ratio is W_2/W_1=0.5 (W_1=20 mm, W_2=10 mm). The volumetric flow rates in the main and branch channels before confluence are Q_1 and Q_2, respectively, and the confluent flow rate ratio Q_2/Q_1 is changed as Q_2/Q_1=1, 2, 3, which correspond to the values of fluid momentum ratio M_2/M_1 of 2, 8, 18, respectively. The value of Q_2/Q_1 is controlled by changing only the volumetric flow rate of the branch channel. The velocity in the main channel is U_1=0.25 m/s, and the velocity in the branch channel is U_2=0.5, 1.0, 1.5 m/s. Reynolds numbers are $Re=(U_3W_1)/\nu$ =1.0×10^4, 1.5×10^4, 2.0×10^4, based on the average velocity U_3 and the width W_1 downstream of the confluent point. Here, ν is the kinematic viscosity of water. Particles are introduced into the branch channel only, using random numbers, so as to satisfy uniform distribution at the volume concentration C_V=0.01. Density and diameter of particles are ρ_p = 2590 kg/m^3 (relative density: ρ_p/ρ_f= 2.59) and d_p=425μm, respectively. Direction of gravity is downward in Fig.9.

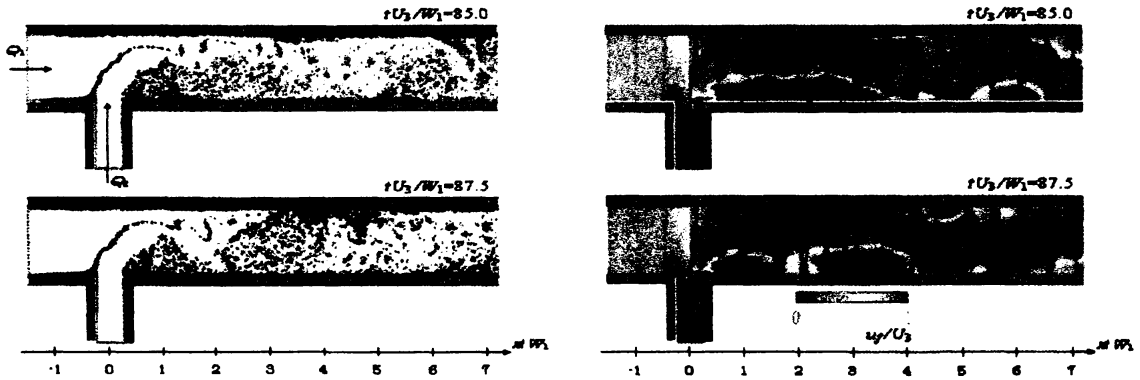

(a) Vortex elements (b) Fluid velocity distributions

Fig.10 Two snap shots of instantaneous distribution of vortex elements and fluid velocities.

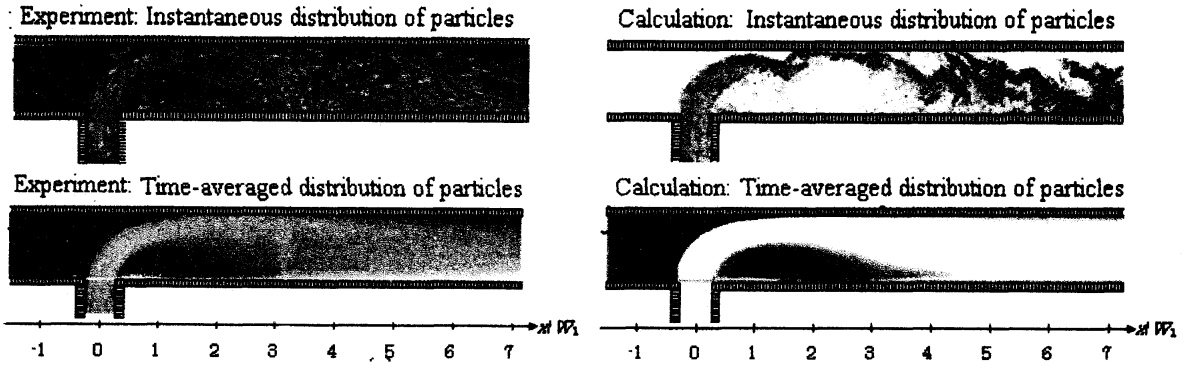

Fig.11 Comparison between calculation and experiment for distribution of particles.

Figure 10 shows two snap shots of instantaneous distributions of vortex elements and fluid velocity obtained by the numerical simulation. The condition of the confluent flow rate ratio is Q_2/Q_1=2, and the instantaneous non-dimensional times are tU_3/W_1=85.0 and 87.5. The contour of velocity expresses the streamwise fluid velocity. After two perpendicular flows merge in the mixing tee, the confluent flow deflects and unsteady flow separation occurs at the downward corner of the junction. First, the confluent flow is accelerated in the contraction region of the mixing point. Then, the flow is decelerated to the streamwise direction in the expansion. Consequently, unsteady flow separation occurs and grows up from the bottom wall of the main channel, because the adverse pressure gradient is strong in the flow direction. The separation vortices aggregate, break up and diffuse downward. Such phenomenon was also observed in the experiments by ink trace visualization.

In Fig.11, the instantaneous and time-averaged distributions of solid particles for the condition of Q_2/Q_1=2 are shown, and numerical results are compared with experimental observations where the time-averaged experimental photographs were taken by long exposure. Both, experimental and numerical results show that particles have mixed almost uniformly at x/W_1=3. As mentioned before, it is seen that the confluent flow deflected and the unsteady separations occurred at the downward corner of the junction. The confluent flow becomes unsteady and complex due to the unsteady separation of flow from the channel walls. Thus, in the condition Q_2/Q_1=2, the ability of the particle mixing is good.

3.3 Plasma particle trajectory tracking method

Expanding the concept of the Lagrangian vortex method in which vorticity layers are expressed by a number of discrete vortex elements, Ishimoto[10] and the group of the present author have attempted numerical simulation of behavior of pure electron plasma in a magnetic field by introducing a number of charged particles called superperticles.

It is known that the motion of non-neutral plasma in a magnetic field is similar to the vortical flow of fluid. So far, formation of coherent vortex structures of two-dimensional electron plasmas have been observed in experiments by Kiwamoto[25]and Sanpei et al.[26], which were performed with the photo-cathode pure-electron plasma traps of a Malmberg-Penning trap type. The vortex crystal formation in two-dimensional plasma turbulence was theoretically investigated by Jin and Dubin[27] and for numerical simulation of the various phenomena in plasma, the particle-in-cell method, the leap-frog method and others are explained by Birdsall and Langdon[28], Naitou[29], Isiguro[30] and Ohsawa[31]. The leap-frog method might be considered the same as the time-splitting method, but a deterministic time-splitting

and Lagrangian method like the advanced vortex element method mentioned above is not discussed in detail, so far.

In general, in a field with the intensity of electric field $\boldsymbol{E}$ and the magnetic density $\boldsymbol{B}$, the motion of a charged particle with the strength of charge q and the mass m is expressed as follows.

$$m\frac{d\boldsymbol{u}}{dt} = q(\boldsymbol{E} + \boldsymbol{u} \times \boldsymbol{B}) \tag{6}$$

Here, $\boldsymbol{u}$ denotes the velocity of the center of the particle which is given by $d\boldsymbol{r}/dt$, and the motion consists of circular motion around the axis of $\boldsymbol{B}$ and the motion of drift in the direction of $\boldsymbol{E}\times\boldsymbol{B}$. In the right-hand side of Eq. (6), the first term $q\boldsymbol{E}$ and the second $q(\boldsymbol{u}\times\boldsymbol{B})$ respectively correspond to the Coulomb force and the Lorentz force acting on the particle. In the study, the two-dimensional motion of superparticles of electrons in a uniform magnetic field $\boldsymbol{B}_0$ was calculated. Therefore, the intensity of electric field $\boldsymbol{E}$ is calculated from the summation of individual intensity of electric field induced by each superparticle in the field and the magnetic density $\boldsymbol{B}$ is given by $(\boldsymbol{B}_0+\mathrm{d}\boldsymbol{B})$ in which $\mathrm{d}\boldsymbol{B}$ denotes fluctuation of magnetic density induced by motions of the electronic superparticles and it is calculated by the Biot-Savart law derived from the Maxwell equation. As the study was a first attempt for the group of the present author to apply the concept of the vortex method, a simple superparticle model was introduced, which has a spherical shape with the radius r_d and the number of electrons uniformly distributed in it is N_v , and to simplify the numerical treatments, the effects of electronic diffusion and collisions between particles were ignored. In order to compare the calculation results with experiments by Kiwamoto[25], the interaction between two clouds of superparticles and the formation of vortex crystals from a ring cloud were calculated under the conditions similar to the experimental ones.

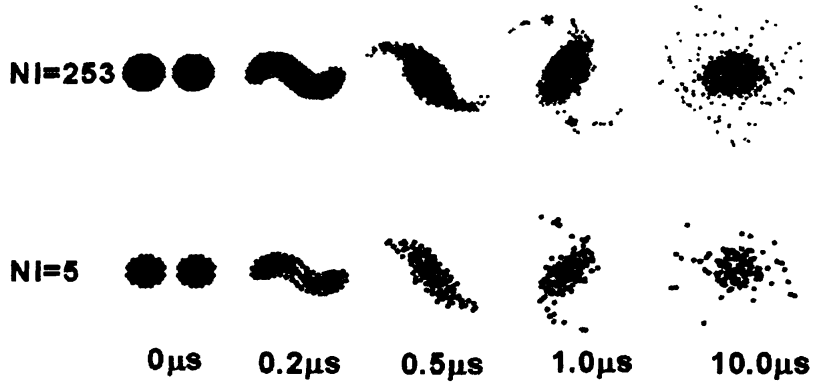

Fig.12 Comparison of calculated results of merging of a pair of electronic plasma.

In the calculations of interaction between two clouds, the following conditions were used; density of magnetic field $\boldsymbol{B}_0$=0.048 N/Am, the charge of an electron e=1.6021× 10^{-19} C, the mass of an electron m_e=9.1091× 10^{-31} kg, the electric permittivity ε_0=8.8542×10^{-12} $C^2/(Nm^2)$, the electric permeability μ =1.2566×10^{-6} N/A^2, the initial radius of a cloud r_i=0.4×10^{-3} m, the initial distance between two clouds L=1.0×10^{-3} m. In order to examine the effect of the number of electrons in a superparticle N_v and the initial number of superparticles in a cloud N_i on the calculation results of evolution of interactive motion of plasmas, a couple of

combinations of the numbers were introduced as (N_v=100, N_i=253) and (N_v=460, N_i=55), and three different values for the radius of superparticle were examined for each combination as r_d =2.5×10^{-5}, 4×10^{-7} and 2.5×10^{-8} m for the case of N_i=253, and r_d=5×10^{-5}, 4×10^{-7} and 5×10^{-8} m for the case of N_i=55. The calculation time step was fixed as dt=1×10^{-10} s.

In Fig.12, a couple of calculation results of evolution of merging of a pair of electronic plasma clouds are shown, which were obtained for (N_i=253, r_d =4×10^{-7} m) and (N_i=55, r_d =4×10^{-7} m). From comparison of the results, it is clearly observed that as the time proceeds, the two clouds catch and join each other, and then they finally merge into a new isolated cloud due to the interactive motion of superparticles. The calculated evolution of merging is in qualitatively coincidence with the experiments[25]. And it has been confirmed that there are no significant differences in the calculated merging processes corresponding to the differences of not only the numbers of both superparticles in a cloud and electrons in a superparticle, but also the radius of a superparticle, as far as this study is concerned.

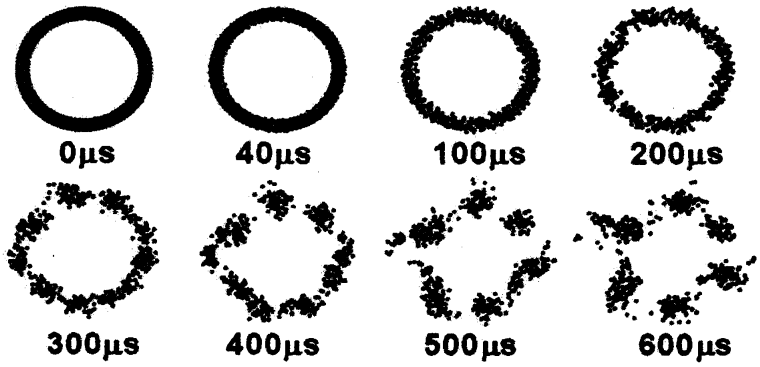

Fig.13 Formation of vortex crystal structure from a ring

In the calculation of the formation of vortex crystals from a ring cloud, the magnetic field conditions are the same as those mentioned above. The initial outer radius and inner radius of the ring cloud are R_o=5×10^{-3} m and R_i=4×10^{-3} m, respectively and the inner radius of the conducting wall in which the ring cloud of plasma was coaxially trapped is R_w=5.5×10^{-3} m. The number of superparticles in the ring cloud is N_r=398 and the number of electrons in a superparticle is N_v=46. In Fig.13, evolution of disturbance on motion of superparticls with time and formation of six vortex crystals are clearly seen. It has been confirmed that the calculated features of vortex crystal formation is also in qualitatively coincidence with the experiments and numerical results reported by Kiwamoto[25].

4. A View of New Direction of Discrete Vortex Dynamics

In the former section, three examples of applications of Lagrangian tracking methods based on a vortex element method and a particle method. It seems very interesting that although the fluid is assumed as continuum and the particles are discrete fragments of a material, the phenomena of vortex formation are certainly observed in dynamic motion of both a fluid and particles. It is well known that the dynamic behaviors of statistically many particles like powder, heavenly bodies in the cosmos, cars on a crowded road, and so on, can be represented by the governing equations in the fluid dynamics. So far, there exist such research fields as powder fluidization, ferrofluid, plasma flow, cosmic fluid, traffic flow and so on, and usually, differential equations of fluid dynamics are applied into investigations of those motions.

However, it must be considered that the applicability of those equations to a microscopically smaller field becomes poorer, because the most of differential equations of

fluid dynamics are constructed for macroscopic flow fields on the assumption of continuum. Therefore, it is not always correct to introduce infinitesimally smaller size of grids in the numerical calculation with use of a huge parallel-computer system aiming to increase accuracy of the numerical treatments.

As shown in the former section, it is important to consider that the introduction of various discrete elements is a key technology of the present numerical treatments, which is common to the calculations of both the dynamic phenomena of vorticity transportation in a fluid and the dynamic motion of particles. In the vortex method, the discrete element is a discrete vortex blob in which the distribution of vorticity and the particle size are modeled. In the particle method used for the two-phase flow calculation, the discrete element is a solid particle itself in which mass and size are modeled. And in the particle method used in the plasma vortex calculation, the discrete element consists of a superparticle in which a distribution of electrons (mass and electric charge) and particle size are modeled. It seems a stimulating fact for consideration of a new direction of discrete vortex dynamics that the vortical phenomena not only in a fluid flow but also in a multi-particle flow can be analyzed by the discrete element method. Although the present author had considered the vortex blobs to be fragments to discretize the continuous vorticity flield, recently he has looked them from a different point of view to be a sort of superparticles, which essentially consists of a number of elementary particles. Therefore, it will be very interesting to accumulate comprehensive knowledge on various kinds of vortex motions from molecular dynamics to cosmetic flow by investigating the fractal features of the vortex motion and by modeling superparticles with various scales and characteristics required in corresponding dynamic fields.

5. Conclusions

In this paper, aiming to overview the recent attempts of progressive application of the advanced vortex method, mathematical background and numerical procedure of the method are briefly explained, and characteristic results of the progressive studies on simulation of complex flows around a 100 m runner, liquid-particle two phase flows in a channel and vortical motion of plasma clouds in a magnetic field are digested with explanation of the particle methods used in the latter two studies. And finally, a new direction of further development of the discrete particle methods for vortex dynamics is discussed. The discussion is summarized as follows.

1) The three examples of applications of the vortex method, the coupled vortex-particle method and the plasma particle method, seem to suggest that most of the vortex motions observed in various fields are essentially oriented to the discrete particle dynamics instead of the continuous fluid dynamics.
2) It is not always correct to introduce infinitesimally smaller size of grids in the numerical calculation with use of a huge parallel-computer system aiming to increase accuracy of the numerical treatments, because the molecular dynamics governs the microscopic field instead of the continuum dynamics.
3) Considering the above discussion, it seems interesting to accumulate comprehensive knowledge on various kinds of vortex motions from molecular dynamics to cosmetic fluid dynamics by investigating the fractal features.
4) It will be a new direction of expansion of the concept of discrete elements methods to establish comprehensive algorithms of modeling physical behaviors of elementary particles like vortex blobs and plasma superparticles which have various scales and physical characteristics required in the corresponding fields.

ACKNOWLEDGMENTS

The author wishes to thank Dr. Ojima of CMH for discussing on the treatment of discrete vortex particles and providing with the software of vortex method used in the calculations of flows around a 100m runner, and Dr. Iso of IHI for discussing on application of the panel methods for internal flows.

REFERENCES

[1] Leonard, A., Vortex methods for flow simulations. *J. Comp. Phys.* 1980, 37, 289-335.

[2]Sarpkaya, T., Computational methods with vortices - the 1988 Freeman scholar lecture. *J. Fluids Engng.*, 1989, 111, 5-52.

[3] Kamemoto, K., On attractive features of the vortex methods. *Computational Fluid Dynamics Review* 1995, ed. M.Hafez and K.Oshima, JOHN WILEY \& SONS, 1995, 334-353.

[4] Kamemoto, K., Recent contribution of an advanced vortex element method to simulation of unsteady vortex flows. *Computational Fluid Dynamics Journal*, 2007, 15(4):55, 422-437.

[5] Ojima A. and Kamemoto, K., Numerical simulation of unsteady flows around a fish. *Proc. of the Third International Conference on Vortex Flows and Vortex Models – ICVFM2005*, Yokohama, Japan, November 2005, 96-101.

[6] Greengard L. and Rohklin V., A fast algorithm for particle simulations. *J. Comp. Phys.* 1987, 73-2, 325-348.

[7] Fukuda K. and Kamemoto, K., Application of a redistribution model incorporated in a vortex method to turbulent flow analysis. *Proc. of the Third International Conference on Vortex Flows and Vortex Models – ICVFM2005*, Yokohama, Japan, November 2005, 131-136.

[8] Kamemoto K. and Ojima A., Application of a vortex method to fluid dynamics in sports science *Proceedings of FEDSM2007 5th Joint ASME/JSME Fluids Engineering Conference*, July30-August 2, 2007 San Diego, California, USA, FEDSM2007-37066.

[9] Iso Y. and Kamemoto K., Vortex method and particle trajectory tracking method for Lagrangian-Lagrangian simulation applied to internal liquid-solid two-phase flows. *Proc. of the Third International Conference on Vortex Flows and Vortex Models – ICVFM2005*, Yokohama, Japan, November 2005, 287-292.

[10] Ishimoto S., Application of vortex method into motional simulation of plasma particles. *Bachelor Thesis, Yokohama National University*, Submitted to Prof. Kamemoto, February 2007.

[11] Wu J.C. and Thompson J.F., Numerical solutions of time-dependent incompressible Navier-Stokes equations using an integro-differential formulation. *Computers & Fluids*, 1973, 1-1, 197-215.

[12] Uhlman, J.S., An integral equation formulation of the equation of motion of an incompressible fluid. *Naval Undersea Warfare Center*, 1992, *T.R.* 10-086.

[13] Ojima A. and Kamemoto K., Numerical simulation of unsteady flow around three dimensional bluff bodies by an advanced vortex method. *JSME Int. Journal*, B, 2000, 43-2, 127-135.

[14] Winkelmans G. and Leonard A., Improved vortex methods for three-dimensional flows. *Proc. Workshop on Mathematical Aspects of Vortex Dynamics*, Leeburg, Virginia, USA, 1988, 25-35,

[15] Nakanishi Y. and Kamemoto K., Numerical simulation of flow around a sphere with vortex blobs. *Journal Wind Eng. and Ind. Aero*, 1992, 46-47, 363-369.

[16] Iso Y. and Kamemoto K., Vortex method and particle trajectory tracking method for liquid-solid two-phase simulation applied to internal flows. *Trans. JSME* Ser.B, 2005, 71-71, 2671-2678, (in Japanese).

[17] Tsuji Y., Morikawa Y., Tanaka T., Nakatsukasa N. and Nakatani M., Numerical simulation of gas-solid two-phase flow in a two-dimensional horizontal channel. *Int. J. Multiphase Flow*, 1987, 13-5, 671-684.

[18] Yamamoto Y., Potthoff M., Tanaka T., Kajishima T and Tsuji Y., Large-eddy simulation of turbulent gas-particle flow in a vertical channel: effect of considering inter-particle collision. *J. Fluid Mech.*, 2001, 442, 303-334.

[19] Dennis, S. C. R, Singh S.N. and Inghan D.B., The steady flow due to a rotating sphere at low and moderate Reynolds number. *J. Fluid Mech.*, 1980, 101, 257-279.

[20] Hishida, K., Hanzawa Y., Sakakibara J., Satou Y. and Maeda M., *Trans of JSME*, Ser. B 1996, 62-593, 18-25 (in Japanese).

[21] Hishida, K., Hanzawa Y., Sakakibara J., Satou Y. and Maeda M., *Trans of JSME*, Ser. B 1996, 62-593, 26-33 (in Japanese).

[22] Kawashima Y., Nakagawa M. and Inoue S., Characteristics of mixing due to confluent flow in a two-dimensional right-angled T-shaped flow section. *The Society of Chemical Engineers Japan*,1982,8-2,109-114, (in Japanese).

[23] Kawashima Y., Nakagawa M. and Inoue S., Flow patterns at a two-dimensional right-angled T-shaped confluence. *The Society of Chemical Engineers Japan*, 1982, 8-6, 664-670, (in Japanese).

[24] Blancard J. N. and Brunet Y., Interaction between a jet getting out of a thin slit and emerging into a cross flow. *ASME Fluids Eng. Div. Conf.*, 1996, 4, 39-46.

[25] Kiwamoto Y., Vortex dynamics in nonneutral plasma. *J. Physical Society of Japan*, 2001, 56-4, 253-261, (in Japanese).

[26] Sanpei A., Ito K., Soga Y., Aoki J. and Kiwamoto Y., Formation of a symmetric vortex configuration in a pure electron plasma trapped with a penning trap. *Hyparfine Interact*, 2007,174,71-76.

[27] Jin D.Z.and Dubin D.H.E., Theory of vortex crystal formation in two-dimensional turbulence. *Phys. Plasmas*, 2000,7-5,1719-1722.

[28] Birdsall C.K. and Langdon A.B. , *Plasma Physics via Computer Simulation* (McGraw-Hill Book Company, New York, 1985 and Adam Hilger, Bristol, Philadelphia and New York, 1991).

[29] Naitou H., Basic theory of particle simulation. *Jr. Plasma and Fusion Research*, 1998, 74 –5, 470-478 (in Japanese).

[30] Ishiguro S., Electrostatic Particle Simulation. *Jr. Plasma and Fusion Research*, 1998, 74 –6, 591-597 (in Japanese).

[31] Ohsawa Y., Relativistic Electromagnetic Particle Simulation. *Jr. Plasma and Fusion Research*, 1998, 74 –7, 746-752 (in Japanese).